Magnetostatic modes of lateral metal magnetic superlattices

Cheng Jia
Department of Physics, Harbin Normal University, Harbin 150080, China

Xuan-Zhang Wang*
CCAST (World Laboratory), P.O. Box 8730, Beijing 10080, China
and Department of Physics, Harbin Normal University, Harbin 150080, China

Shu-Chen Lü
Department of Physics, Harbin Normal University, Harbin 150080, China
(Received 11 March 1999; revised manuscript received 9 September 1999)

We investigate magnetostatic modes of lateral magnetic superlattices composed of metallic magnetic layers and insulating nonmagnetic layers, with an effective-medium theory. We assume that the in-plane waves always propagate normal to the static magnetization for an arbitrary external field applied parallel to the surface, and that the damping results from eddy currents. Some particular features of the frequency and damping are seen, for example, the damping is not the lowest for a higher applied field vertical to the magnetic-nonmagnetic layers, but it is the lowest for a smaller applied field. These features of the frequency and damping are not only governed by the conductivity and wave number, but also by the direction and magnitude of external magnetic field. The patterns of obtained calculation curves are complicated. Our results in the limiting case of conductivity $\sigma=0$ are consistent with those in the previous works. The numerical calculations are presented for the Ni-vacuum superlattice.

I. INTRODUCTION

Nowadays an interesting field has been formed in the study of spin-wave dispersion properties in gyromagnetic mediums, especially in ferromagnets and antiferromagnets. According to the wave number of spin waves, the range of the spectrum can be divided roughly into four regions (exchange, dipole-exchange, magnetostatic, and electromagnetic), and the modes of the spin waves in each of these regions can be determined and detected with particular theories and variant experimental techniques.[1–3] While investigating the dispersion relations of the spin-wave modes in the magnetostatic and electromagnetic regions, dampings is usually omitted, and this is practically feasible in the case of insulating magnets with a perfectly crystal structure and at low temperature. Recently, the authors of Ref. 4 advanced some discussions concerning the effects of eddy currents on the reflection of electromagnetic radiation from a lateral metallic magnetic superlattice film. In this reference, due to the presence of the insulating spacers the electron motion is limited in a certain direction, so that those features can be found from the magnetic excitations of the metallic magnetic system. More recently, in a discussion of influences of eddy currents upon the magnetostatic modes in ferromagnets,[5] the influences are proved to be more obvious when the ferromagnets are metallic. The conductivity of metallic magnets like Ni and Fe is so high, that the imaginary part (it is related to the eddy currents) of the complex dielectric coefficient is much larger than its real part, which can be omitted naturally. As a result, the question enters into the field to study the magnetostatic modes of metallic magnets. In the electromagnetic region of spin waves, the retarded modes of antiferromagnets are more practically interesting. The recent experiments of the attenuation total reflection on the antiferromagnet FeF_2 show that some features of the retarded modes, especially the nonreciprocity of the surface modes, can be identified more precisely and the experimental results are consistent with the theoretical ones.[6,7] In our last paper,[8] we discussed the effects of eddy currents in noninsulating antiferromagnets with a uniaxial anisotropy on the retarded modes which requires an equal importance of both the real part and imaginary part of the complex dielectric coefficient.

The superlattice used in this paper is similar to that in Ref. 4, composed of metallic ferromagnetic layers and insulating nonmagnetic layers. In contrast to Ref. 4, where the reflection of electromagnetic radiation from the system was discussed, our aim is to investigate the dispersion properties of magnetostatic waves. We propose that the damping results completely from eddy currents in the superlattice, and the direction and magnitude of the external magnetic field in the surface of the superlattice can be changed. For simplicity, we choose a geometry similar to the Voigt geometry, in which the wave propagates transversely to the static magnetization and along the surface. Of course, the direction of the magnetization changes with both the direction and magnitude of the field, due to the presence of the demagnetizing field.

II. THEORY

We studied magnetostatic and retarded modes in some high-symmetry configurations in Refs. 9–12, where the static magnetization is always parallel to the applied field. For the investigation of magnetostatic modes, the direction of the in-surface wave vector can be changed and there is a critical propagation angle of surface modes. For studies of retarded modes, one always takes the Voigt geometry, where the

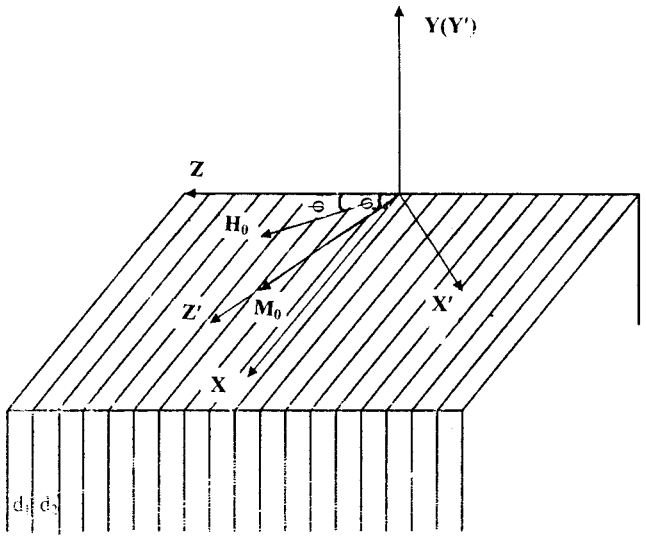

FIG. 1. Geometry considered in this paper. The applied field $\mathbf{H_0}$ makes an angle φ and the static magnetization $\mathbf{M_0}$ (along the z' axis) makes another angle φ' with respect to the z axis normal to the magnetic-nonmagnetic layers. The wave always propagates along the x' axis normal to the magnetization, or say the z' axis. The x-z or x'-z' plane is the surface of the superlattice. The y or y' axis is perpendicular to the surface. d_1 and d_2 are the thicknesses of the magnetic and nonmagnetic layers.

wave vector is normal to the magnetization and applied field. We also discussed the magnetostatic modes in a low-symmetry geometry,[13] where the direction of an applied static field can be changed. In this paper, we consider a more general configuration, i.e., the applied field $\mathbf{H_0}$ makes any angle φ with respect to the axis z transverse to the magnetic-nonmagnetic layers (see Fig. 1). Due to the presence of the demagnetizing field, the static magnetization $\mathbf{M_0}$, generally speaking, is not parallel to $\mathbf{H_0}$, so we assume that it makes the angle φ' with respect to the z axis. If the direction or magnitude of $\mathbf{H_0}$ is changed, the angle φ' varies. In theoretical derivation we also need the other coordinate system with the z' axis parallel to $\mathbf{M_0}$, the x' axis in the surface and the y' axis parallel to the y axis. The wave always propagates along the x' axis. d_1 and d_2 indicate the widths of the ferromagnetic and nonmagnetic layers, so that $D=d_1+d_2$ is the superlattice period. As before,[9–13] we employ the effective-medium approximation which means that the superlattice is described as a homogeneous anisotropic medium with an averaged magnetic permeability tensor and complex dielectric coefficient tensor.

First, the effective-medium permeability of the superlattice is given by[13]

$$\vec{\mu}'^{e}=\begin{pmatrix} \mu_{11} & i\mu_{12} & 0 \\ -i\mu_{21} & \mu_{22} & 0 \\ 0 & 0 & 1 \end{pmatrix}, \tag{1}$$

where

$$\mu_{11}=[\mu+(f_2+f_1\mu)c\tan^2\varphi']/(f_1+f_2\mu+c\tan^2\varphi'), \tag{2a}$$

$$\mu_{22}=f_2+f_1\mu-f_1f_2\mu_\perp^2/(f_1+f_2\mu+c\tan^2\varphi'), \tag{2b}$$

$$\mu_{12}=\mu_{21}=f_1\mu_\perp(1+c\tan^2\varphi')/(f_1+f_2\mu+c\tan^2\varphi') \tag{2c}$$

with $f_1=d_1/D$, $f_2=d_2/D$, and

$$\mu=1+\omega_i\omega_m/(\omega_i^2-\omega^2), \tag{3a}$$

$$\mu_\perp=\omega_m\omega/(\omega_i^2-\omega^2), \tag{3b}$$

in which $\omega_m=4\pi\gamma M_0$ and

$$\omega_i=\gamma[H_0^2\sin^2\varphi+(H_0\cos\varphi-4\pi M_0\cos\varphi')^2]^{1/2}. \tag{4}$$

The relation between φ and φ' in formula (4) is

$$\tan\varphi'=\frac{H_0\sin\varphi}{H_0\cos\varphi-4\pi M_0\cos\varphi'}. \tag{5}$$

For $\varphi=90°$ and $0°$, the static field and magnetization have the same direction. At $\varphi=90°$, the demagnetizing field vanishes and it reaches its maximum at $\varphi=0°$.

Second, we derive the expression of the effective-medium dielectric coefficient tensor in the $x'y'z'$ coordinate system from that in the xyz system. In the xyz coordinate system[4]

$$\vec{\varepsilon}=\begin{pmatrix} \varepsilon_{xx}=f_1\varepsilon_1+f_2\varepsilon_2 & 0 & 0 \\ 0 & \varepsilon_{yy}=f_1\varepsilon_1+f_2\varepsilon_2 & 0 \\ 0 & 0 & \varepsilon_{zz}=\dfrac{\varepsilon_1\varepsilon_2}{f_1\varepsilon_2+f_2\varepsilon_1} \end{pmatrix}, \tag{6}$$

where ε_2 is the dielectric constant of the nonmagnetic layers, and ε_1 is the complex dielectric coefficient of the magnetic layers, given by

$$\varepsilon_1=\varepsilon_0\left(\varepsilon_r+i\frac{\sigma}{\varepsilon_0\omega}\right). \tag{7}$$

In formula (7), ε_0 represents the vacuum dielectric constant, ε_r is the relative dielectric constant, and σ is the electrical conductivity. Thus the effective-medium dielectric coefficient tensor in the $x'y'z'$ coordinate system can be written as

$$\vec{\varepsilon}'^{e}=T\vec{\varepsilon}^{e}T^{-1}, \tag{8}$$

where the transformation matrix T is defined as

$$T=\begin{pmatrix} \cos\varphi' & 0 & -\sin\varphi' \\ 0 & 1 & 0 \\ \sin\varphi' & 0 & \cos\varphi' \end{pmatrix}. \tag{9}$$

After the substitution of Eq. (9) into Eq. (8), we have

$$\vec{\varepsilon}'^{\,e}=\begin{pmatrix} \varepsilon_{11} & 0 & \varepsilon_{13} \\ 0 & 1 & 0 \\ \varepsilon_{31} & 0 & \varepsilon_{33} \end{pmatrix} \tag{10}$$

with

$$\varepsilon_{11}=\varepsilon_{xx}\cos^2\varphi'+\varepsilon_{zz}\sin^2\varphi', \tag{11a}$$

$$\varepsilon_{33}=\varepsilon_{xx}\sin^2\varphi'+\varepsilon_{zz}\cos^2\varphi', \tag{11b}$$

and

$$\varepsilon_{13}=\varepsilon_{31}=\sin\varphi'\cos\varphi'(\varepsilon_{xx}-\varepsilon_{zz}). \tag{11c}$$

In two special geometries, $\varphi=90°$ and $0°$, matrix (10) is diagonal. Because $\sigma/(\varepsilon_0\omega)\gg\varepsilon_r$ in Eq. (7) for the metallic ferromagnetic layers, and we are interested in investigating magnetostatic modes, the displacement current terms are ignored on the right-hand side of the equation

$$\nabla'\times\mathbf{h}=\frac{\partial}{\partial t}(\vec{\varepsilon}'^{\,e}\cdot\mathbf{e}) \tag{12}$$

but the conduction current terms are preserved, which leads to

$$\nabla'\times\mathbf{h}=\vec{\sigma}'^{\,e}\cdot\mathbf{e}, \tag{13}$$

where $\mathbf{e}$ is the induced electric field. According to Eqs. (7) and (11), the nonzero components of the effective conductivity tensor $\vec{\sigma}'^{\,e}$ are presented as follows:

$$\sigma_{11}=f_1\sigma(1-F\sin^2\varphi'), \tag{14a}$$

$$\sigma_{22}=f_1\sigma, \tag{14b}$$

$$\sigma_{33}=f_1\sigma(1-F\cos^2\varphi'), \tag{14c}$$

and

$$\sigma_{13}=\sigma_{31}=f_1\sigma\sin\varphi'\cos\varphi' F \tag{14d}$$

with

$$F=1-\frac{\varepsilon_2^2}{[(f_1\varepsilon_2+f_2\varepsilon_0\varepsilon_r)^2+(f_2\sigma/\omega)^2]}. \tag{15}$$

On the above bases, we can derive the dispersion relations of the magnetostatic waves in the superlattice with the eddy currents. Since the main formulas (1), (10), and (13) are all given in the $x'y'z'$ coordinate system, the derivation of dispersion relations will be carried out in this system.

The derivation of the dispersion relations is different from those in Refs. 1 and 9–13. First, the term on the right-hand side of Eq. (13) is not zero so that we cannot introduce a magnetostatic potential to describe the real physical fields. Second, the tensor $\vec{\sigma}'^{\,e}$ included in Eq. (13) is not diagonal. In the $x'y'z'$ coordinate system, we introduce a formal solution of the field

$$\mathbf{h}=\mathbf{h}\exp(ikx'+\alpha y'-i\omega t)\quad (y'<0), \tag{16a}$$

$$\mathbf{h}=\mathbf{h}_0\exp(ikx'-ky'-i\omega t)\quad (y'>0). \tag{16b}$$

In Eqs. (16), k is the wave number. α can be a complex number, and its real part is the decay coefficient of the wave in the superlattice, but above this superlattice the decay coefficient is equal to k.

Applying solution (16a), Eqs. (13) and

$$\nabla'\times\mathbf{e}=-\frac{\partial}{\partial t}(\vec{\mu}'^{\,e}\cdot\mathbf{h}), \tag{17}$$

we obtain

$$\alpha h_z=\sigma_{11}e_x+\frac{i\sigma_{13}\omega}{\alpha}(\mu_{11}h_x+i\mu_{12}h_y), \tag{18a}$$

$$h_z=\sigma_{22}k^{-2}(\omega h_z-i\alpha e_x), \tag{18b}$$

$$ikh_y-\alpha h_x=\sigma_{13}e_x+\frac{i\omega\sigma_{33}}{\alpha}(\mu_{11}h_x+i\mu_{12}h_y), \tag{18c}$$

and

$$ik(\mu_{11}h_x+i\mu_{12}h_y)=\alpha(i\mu_{12}h_x-\mu_{22}h_y), \tag{18d}$$

where Eq. (18d) results from $\nabla\cdot\mathbf{b}=0$. These four equations result in an equation satisfied by α, that is

$$i\omega\sigma_{13}^2\mu_v(\sigma_{22}\omega+ik^2)+(i\sigma_{22}\alpha^2-\sigma_{11}\sigma_{22}\omega-i\sigma_{11}k^2)\times\left(i\omega\sigma_{33}\mu_v+\alpha^2-\frac{\mu_{11}k^2}{\mu_{22}}\right)=0, \tag{19}$$

where $\mu_v=(\mu_{11}\mu_{22}-\mu_{12}^2)/\mu_{22}$. We see from Eq. (19) that there are two different solutions of α, called α_1 and α_2, which correspond to two different eigenmodes, respectively. Thus this superlattice is birefringent. The presence of different solutions of α can also be found by studying the dipole-exchange modes in magnetic films.[1] The wave function $\mathbf{h}$ in the superlattice should be a linear combination of these two mode functions. Then the wave field $\mathbf{h}$ for $y'<0$ should be rewritten as

$$\mathbf{h}=[\mathbf{h}_1\exp(\alpha_1 y')+\mathbf{h}_2\exp(\alpha_2 y')]\exp(ikx'-i\omega t). \tag{20}$$

This formula and Eq. (16b) will be used when the boundary conditions are employed to find the dispersion equation. Above the superlattice ($y'>0$), $\nabla\times\mathbf{h}=0$. We should mention that $\mathrm{Re}(\alpha_1)>0$ and $\mathrm{Re}(\alpha_2)>0$ for the physical solutions. Further using Eqs. (18a)–(18d) to find the expressions of $\beta_i=h_{iy}/h_{iz}$ and $\gamma_i=h_{ix}/h_{iz}$, one finds

$$\beta_i=\frac{1}{\omega\sigma_{22}\sigma_{13}\alpha_i\mu_v\mu_{22}}(\alpha_i\mu_{12}-k\mu_{11})\times[\alpha_i^2\sigma_{22}+\sigma_{11}(i\omega\sigma_{22}-k^2)], \tag{21a}$$

$$\gamma_i=\frac{1}{i\omega\sigma_{22}\sigma_{13}\alpha_i\mu_v\mu_{22}}(\alpha_i\mu_{22}-k\mu_{12})$$
$$\times[\alpha_i^2\sigma_{22}+\sigma_{11}(i\omega\sigma_{22}-k^2)]. \quad (21b)$$

The use of the boundary conditions at the surface of the superlattice results in an equation

$$\mu_{22}(\beta_2-\beta_1)+i(1+\mu_{12})(\gamma_1-\gamma_2)=0. \quad (22)$$

Substituting formulas (21a) and (21b) into Eq. (22), one finds the final dispersion relation

$$\alpha_1\alpha_2\sigma_{22}[\mu_{22}(\alpha_1+\alpha_2+\mu_v k)-k\mu_{12}]+\sigma_{11}k(k^2-i\omega\sigma_{22})$$
$$\times(\mu_{22}\mu_v-\mu_{12})=0. \quad (23)$$

From the dispersion relations (23) and (19), we know that $\omega=\Omega+i\Gamma$ is complex and its real part is the mode frequency and the imaginary part represents the damping. There are two interesting geometries, one corresponds to $\varphi=0°$ and the other to $\varphi=90°$. In these geometries, α_1 and α_2 are shown by

$$\alpha_1^2=\frac{\mu_{11}}{\mu_{22}}k^2-i\omega\sigma_{33}\mu_v, \quad (24a)$$

$$\alpha_2^2=\frac{\sigma_{11}}{\sigma_{22}}k^2-i\omega\sigma_{11}, \quad (24b)$$

and the dispersion relation is simplified as

$$\alpha_1\mu_{yy}+k\mu_v-k\mu_{xy}=0. \quad (25)$$

The eddy current influences the dispersion properties only through σ_{33}. One can find that σ_{33} increases with ω or σ in the geometry of $\varphi=0°$. Since we have proposed that the damping results from the eddy current, the damping also increases with ω or σ. For the geometry of $\varphi=90°$, $\sigma_{33}=f_1\sigma$, and we see only the influence of the eddy current on the damping that increases with σ. The change of damping with ω can be seen from numerical calculations for the dispersion relation. The expression of σ_{33}, formula (14c) with expression (15), shows us that the effective conductivity is much lower in the first geometry than the second, which proves that the motion of electrons is limited effectively in the first geometry, so the energy loss of the waves should be lower.

III. NUMERICAL RESULTS AND DISCUSSION

We take the Ni-vacuum superlattice as an example for numerical calculations, in which the Ni layers are metallic and ferromagnetic, but the vacuum spacers are insulating and nonmagnetic. The motion of electrons along the direction normal to the layers is limited, and furthermore, one may see some features of magnetic excitons or polaritons of metallic magnets from the reflection of magnetoelectric radiation.[4] The parameters used in the numerical calculation are $4\pi M_0=6.032$ kG, $\gamma=1.93\times10^7$, and $\sigma=1.46\times10^7\ \Omega^{-1}\ \mathrm{m}^{-1}$. Frequencies and damping are quoted in kG with the conversion 1 kG=3.072 GHz. For Ni layers, $\sigma/(\varepsilon_0\omega)\gg1$ so that the displacement current term is omitted in Eq. (12) and the conduction current term has obvious effects on the magnetostatic modes. For simplicity we choose the propagation direction of the magnetostatic mode perpendicular to the magnetization and along the x' axis. This geometry is similar to the Voigt geometry used in previous papers.

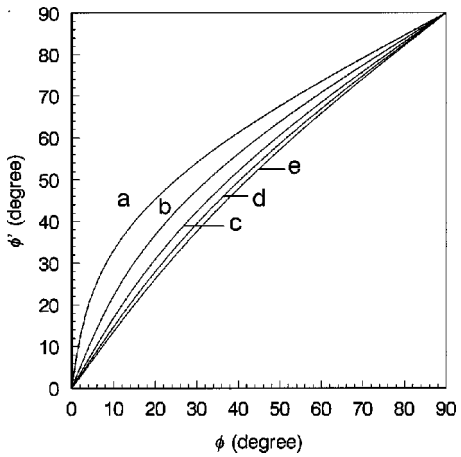

FIG. 2. The direction of the magnetization versus that of the applied field for different values of the field. Curves (a)–(e) correspond to $H_0=6.10$, 7.0, 14.0, 21.0, and 28.0 kG, respectively.

Because the direction of the applied field $\mathbf{H_0}$ can be changed, generally speaking, the magnetization $\mathbf{M_0}$ and the applied field $\mathbf{H_0}$ do not have the same direction as the demagnetizing field exists. $\mathbf{M_0}$ is directed along $\mathbf{H_0}$ in two limit cases, or the applied field is normal to the layers (along the z axis) and it is parallel to the layers (along the x axis). Figure 2 illustrates numerically the direction angle of the magnetization as a function of the direction of $\mathbf{H_0}$ for different values of the field. We can imagine that $\mathbf{M_0}$ is parallel to $\mathbf{H_0}$ when $H_0\to\infty$, but a larger difference is seen for a smaller value of H_0, where φ and φ' are the direction angles of $\mathbf{H_0}$ and $\mathbf{M_0}$, respectively.

In our assumption, the damping and the mode frequency may be modified obviously in the presence of eddy currents. The eddy currents are induced by the electric field of the mode. For different propagation directions, the strength and direction of this field are different. The motion of electrons, however, is limited only in the direction of the z axis. Thus the mode frequency and damping must be related to the propagation direction of the magnetostatic waves. We present the frequency and damping versus the direction of $\mathbf{H_0}$ in Fig. 3, where the wave number is fixed at $k=3.0\times10^4\ \mathrm{m}^{-1}$). From Fig. 3(a) one sees that for $H_0=7.0$ kG the frequency and damping are the lowest when the field $\mathbf{H_0}$ is normal to the layers, or say $\varphi=\varphi'=0°$ and are the highest as $\mathbf{H_0}$ is parallel to the layers ($\varphi=\varphi'=90°$). However, Fig. 3(b) shows that for $H_0=14.0$ kG the frequency is the lowest at about $\varphi=30°$, but the damping is the lowest at about $\varphi=20°$. One also finds that the frequency and damping do not change monotonously with the direction of the applied field.

In Fig. 4, we present the damping as a function of wave number for $H_0=7.0$ kG. The damping decreases first, and then increases as the wave number is increased for smaller angles of the field, but it increases monotonously with the wave number for larger angles. We also see that the damping is the lowest at $\varphi=0°$ and the highest at $\varphi=90°$. This point is the same as that obtained in Fig. 3 and the above section.

Now we show the mode frequency as a function of the

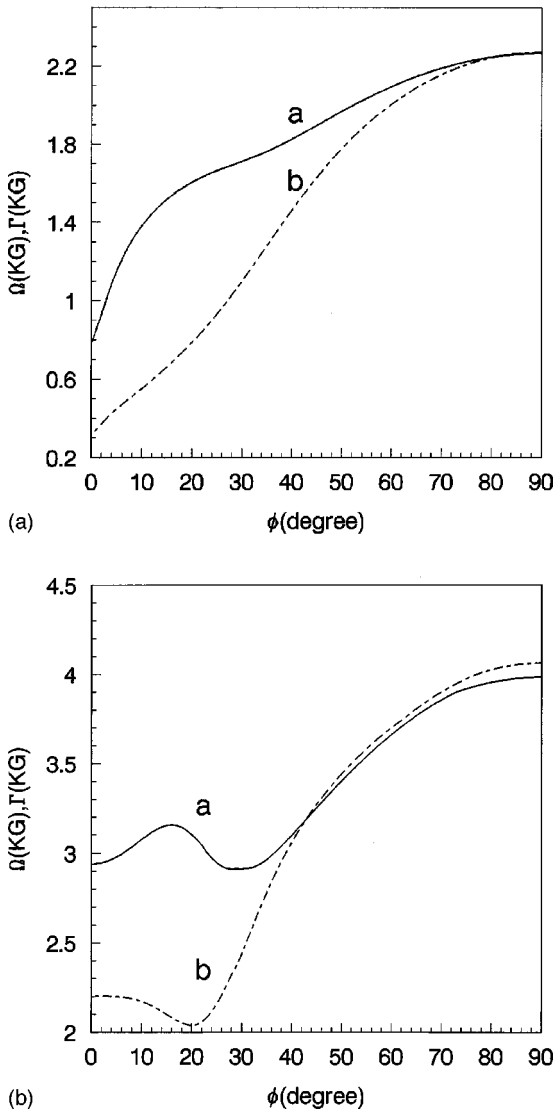

FIG. 3. Frequency and damping of the mode versus the direction of the applied field for $f_1=0.8$ and the wave number $k=3.0$. (a) $H_0=7.0$ kG, and (b) $H_0=14.0$ kG. The solid curves represent the frequency function and the dashed curves show the damping.

wave number for different direction angles where the field is fixed at 7.0 or 14.0 kG. Figure 5(a) corresponding to $H_0=7.0$ kG, shows that the frequency always increases as the direction angle of the field is increased and those curves for $\varphi>30°$ have the smallest value, but the other curves show the frequency increase with the wave number. For a higher field $H_0=14.0$ kG, Fig. 5(b) shows that except for some of the characters presented in Fig. 5(a), there are other new features. The mode frequency increases faster for a small direction angle than a large direction angle of $\mathbf{H_0}$, and the frequency of curve *c* related to $\varphi=20°$ is the lowest at the limit of small wave numbers. In addition, in the range of large wave numbers, the frequency increases as the direction angle of $\mathbf{H_0}$ is decreased, but for curve *c* $\varphi=20°$ is still an exception and it is below curves *a* and *b* related to $\varphi=0°$ and 10°.

Comparing the present numerical results with those obtained without conductivity also is interesting. For $\sigma=0$, our mode becomes the surface magnetostatic mode because we

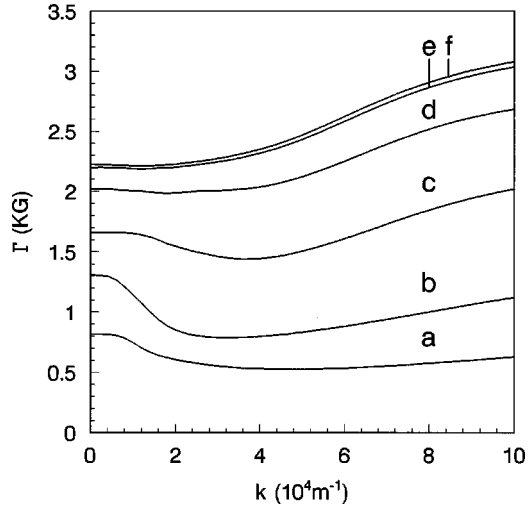

FIG. 4. Damping as a function of wave number for different directions of the field for $f_1=0.8$ and $H_0=7.0$ kG. Curves (a)–(f) are related to $\varphi=10°$, 20°, 40°, 60°, 80°, and 90°, respectively.

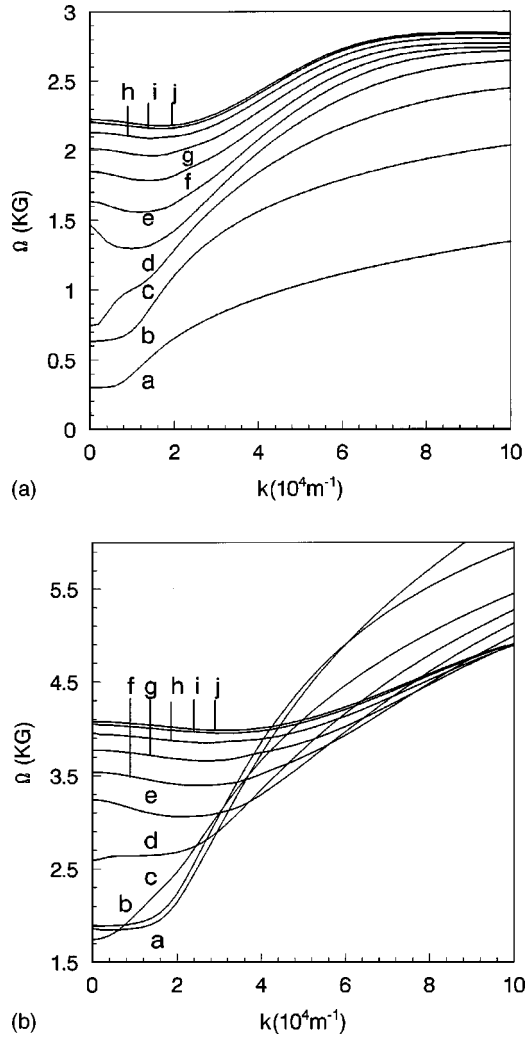

FIG. 5. Frequency as a function of wave number for $f_1=0.8$ and different directions of the field. (a) $H_0=7.0$ kG, and (b) $H_0=14.0$ kG. Curves (a)–(j) are related to $\varphi=0°$, 10°, 20°, . . . , 70°, 80°, and 90°, respectively.

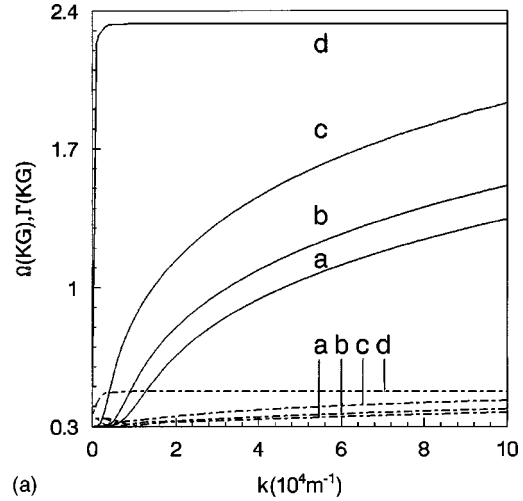

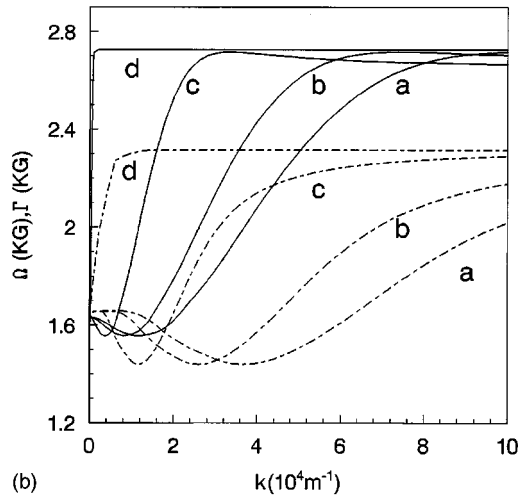

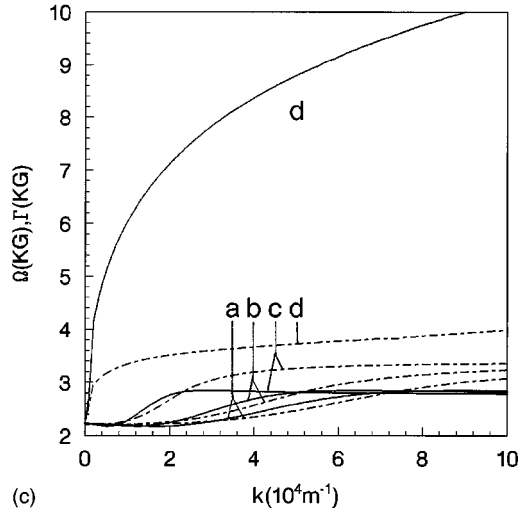

FIG. 6. Frequency and damping versus wave number for $H_0=7.0\,\mathrm{kG}$, $f_1=0.8$, and the field angle equal to (a) $\varphi=0°$, (b) $\varphi=40°$, and (c) $\varphi=90°$. Curves (a)–(d) correspond to $\sigma=1.46\times10^7$, 0.73×10^7, 1.46×10^6, and $1.46\ \Omega^{-1}\,\mathrm{m}^{-1}$. The solid curves show the frequency and the dashed curves represent the damping.

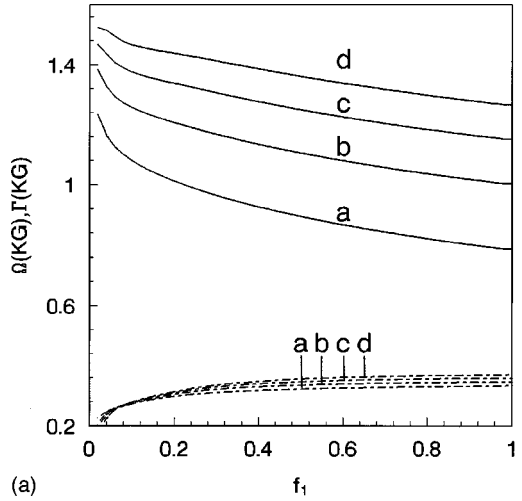

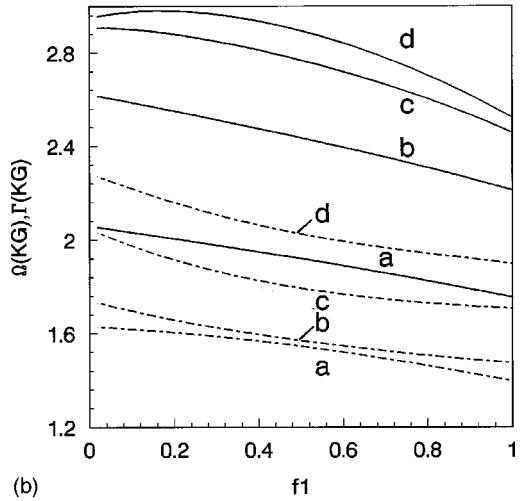

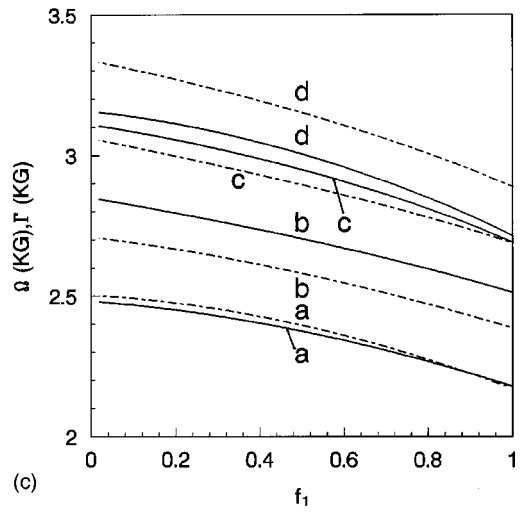

FIG. 7. Frequency and damping versus magnetic faction f_1 for $H_0=7.0\,\mathrm{kG}$, $\sigma=1.46\times10^7\,\Omega^{-1}\,\mathrm{m}^{-1}$ and the field angle equal to (a) $\varphi=0°$, (b) $\varphi=40°$, and (c) $\varphi=90°$. Curves (a)–(d) are related to wave number $k=3.0\times10^4\,\mathrm{m}^{-1}$, $5.0\times10^4\,\mathrm{m}^{-1}$, $7.0\times10^4\,\mathrm{m}^{-1}$, and $9.0\times10^4\,\mathrm{m}^{-1}$. The solid curves show the frequency and the dashed curves show the damping.

have $\mathrm{Re}(\alpha)>0$ and $\mathrm{Im}(\alpha)=0$ in this case. In order to see the effects of conductivity on the magnetostatic waves, in Fig. 6 we present the frequency and damping as a function of wave number for different values of conductivity σ and field angle φ. For $\varphi=0°$ Fig. 6(a) shows that the frequency and damping increase as σ is decreased and they almost do not change with the wave number for a very small conductivity, which corresponds to a feature of the magnetostatic modes in rel-

evant systems without damping. The damping begins to decrease as the conductivity is decreased further from $\sigma = 1.46\ \Omega^{-1}\,\mathrm{m}^{-1}$. For $\sigma = 0$ the frequency is 3.4 kG that is consistent with that given by Fig. 3(a) in Ref. 11, where eddy currents and damping are ignored. For keeping the figure clear, some curves with very small conductivity are not put in it. For $\varphi = 40°$, Fig. 6(b) shows that the frequency and damping have the smallest value in the region of low wave number. Comparing Fig. 6(b) with 6(a) the damping is higher so that eddy currents are stronger for this angle. For $\sigma = 0$, the damping vanishes and frequency does not change with wave number. For $\varphi = 90°$, the demagnetizing field does not exist so that the frequency becomes high, especially for smaller values of σ, and the frequency $\Omega = 10.8\,\mathrm{kG}$ for $\sigma = 0$. This value also can be obtained from Fig. 3 in Ref. 16, where conductivity and damping are ignored.

For a magnetic superlattice, the properties also can change with the magnetic faction f_1. Figure 7 illustrates the frequency and damping versus f_1 for different values of wave number and at a fixed angle of the field. When the field is perpendicular to the layers, or $\varphi = 0°$ [see Fig. 7(a)] the frequency decreases and the damping increases as f_1 is increased. For the field with $\varphi = 40°$ or 90° [see Figs. 7(b) and 7(c)] a different feature is that the damping lowers as the magnetic faction is heightened. From Fig. 7 we see more clearly that the damping is very low when the field is transverse to the layers.

IV. SUMMARY AND CONCLUSIONS

We have investigated magnetostatic modes of a ferromagnetic-nonmagnetic superlattice with a lateral surface, where magnetic layers are metallic, but nonmagnetic layers are insulating. In our calculations we assume the wave vector always is normal to the static magnetization, and the effects of eddy current and demagnetizing field are included.

Some interesting features of the magnetostatic modes are found. First, for a lower applied field ($H_0 = 7.0\,\mathrm{kG}$), the wave frequency and damping is the lowest when the applied field is perpendicular to the magnetic or nonmagnetic layers of the superlattice, and the highest when the field is parallel to the layers. For a higher field ($H_0 = 14.0\,\mathrm{kG}$), the lowest values of the frequency and damping are not at the field angle $\varphi = 0°$. In addition, the frequency and damping curves are very distinctive [see Fig. 3(b)]. Second, for $H_0 = 7.0\,\mathrm{kG}$, the mode frequency always is lower for a lower field angle than for a higher field angle, but for $H_0 = 14.0\,\mathrm{kG}$ the situation is completely different [to compare Fig. 5(a) with Fig. 5(b)]. Third, for the applied field transverse to the layers, the damping increases with the magnetic faction, but for the field parallel to the layers the damping decreases as the faction is increased. For the conductivity $\sigma = 0$, the damping vanishes, then our results are consistent with those in previous papers on relevant systems without damping and eddy currents.[11,16] In Ref. 4, the authors investigate reflection of electromagnetic radiation from the metallic magnetic multilayers with a structure the same as that used in this paper, but we study the dispersion relation and properties of magnetostatic modes, and we use such a geometry with an applied field of arbitrary direction. The properties of magnetostatic modes of this layered metallic magnetic system may be seen with the optical technologies. We have seen some practical systems,[14,15] produced by patterning magnetic films with the laser interference lithography, which are similar to the superlattice in this paper, but our superlattice is semi-infinite. Of course, it is more interesting that magnetostatic modes of these practical systems are discussed, and the relevant works have been started.

ACKNOWLEDGMENTS

The work was supported by the National Natural Science Foundation of China with Grant No. 19574014, the Outstanding Youth Science Foundation, and Natural Science Foundation of Heilongjiang Province, China.

*Author to whom correspondence should be addressed: Xuan-Zhang Wang, Department of Physics, Harbin Normal University, Harbin 150080, China.

[1] M. G. Cottam and D. R. Tilley, *Introduction to Surface and Superlattice Excitations* (Cambridge University Press, Cambridge, 1989).

[2] Kamsul Abraha and D. R. Tilley, Surf. Sci. Rep. **24**, 125 (1996).

[3] J. R. Ducher, *Linear and Nonlinear Spin Waves in Magnetic Films and Superlattices* edited by M. G. Cottam (World Scientific, Singapore, 1994), Chap. 6.

[4] R. E. Camley, T. J. Parker, and S. R. P. Smith, Phys. Rev. B **53**, 5481 (1996).

[5] N. S. Almeida and D. L. Mills, Phys. Rev. B **53**, 12 232 (1996).

[6] M. R. F. Jensen, T. J. Parker, Kamsul Abraha, and D. R. Tilley, Phys. Rev. Lett. **75**, 3756 (1995).

[7] D. E. Brown, T. Dumelow, T. J. Parker, Kamsul Abraha, and D. R. Tilley, Phys. Rev. B **49**, 12 266 (1994).

[8] Cheng Jia, Xuan-Zhang Wang, and Shu-Chen Lu, Phys. Rev. B **59**, 3310 (1999).

[9] Xuan-Zhang Wang and D. R. Tilley, Phys. Rev. B **50**, 13 472 (1994).

[10] Xuan-Zhang Wang and D. R. Tilley, Phys. Rev. B **52**, 13 353 (1995).

[11] Xuan-Zhang Wang and D. R. Tilley, J. Phys.: Condens. Matter **9**, 5777 (1997).

[12] Hong Gao and Xuan-Zhang Wang, Phys. Rev. B **55**, 12 424 (1997).

[13] Shu-Chen Lü, Xuan-Zhang Wang, and D. R. Tilley, Phys. Rev. B **55**, 12 402 (1997).

[14] B. Hillebrands, S. O. Demokritov, C. Mathieu, S. Riedling, O. Buttner, A. Frank, B. Roos, J. Jorzick, A. N. Slawin, B. Bartenlian, C. Chappert, F. Rousseaux, D. Decanini, E. Cambril, A. Muller, and U. Hartmann, Jpn. J. Appl. Phys. (to be published).

[15] C. Mathieu, J. Jorzick, A. Frank, S. O. Demokritov, B. Hillebrands, A. N. Slawin, B. Bartenlian, C. Chappert, D. Decanini, F. Rousseaux, and E. Cambril, Phys. Rev. Lett. **81**, 3968 (1998).

[16] Xuan-Zhang Wang and D. R. Tilley, Phys. Lett. A **187**, 325 (1994).